

## Article

# A Study on the Effect of Initial Temperature on Combustion Characteristics of RDX Based on the Optical Diagnosis Methods

Zhiyu Yan <sup>1</sup>, Chen Song <sup>1</sup>, Qianqian Li <sup>1,\*</sup>, Yulei Niu <sup>2</sup>, Jinhua Wang <sup>1</sup> and Zuohua Huang <sup>1</sup>

<sup>1</sup> State Key Laboratory of Multiphase Flow in Power Engineering, Xi'an Jiaotong University, Xi'an 710049, China; yanzhiyu28@stu.xjtu.edu.cn (Z.Y.); sch135236@stu.xjtu.edu.cn (C.S.); jinhuawang@xjtu.edu.cn (J.W.); zhhuang@xjtu.edu.cn (Z.H.)  
<sup>2</sup> Xi'an Modern Chemistry Research Institute, Xi'an 710065, China; nyl521@163.com  
\* Correspondence: qianqianli@mail.xjtu.edu.cn

**Abstract:** The purpose of this work is to investigate the effect of different initial temperatures on the combustion characteristics of RDX materials. In the experiments, the electric heating plate below the RDX samples was controlled so that the initial temperatures were set to be 298, 323, 373, 423, and 473 K (below the material melting point), respectively. Three optical diagnostic methods were employed to capture the ignition process, flame thermal radiation, and NO distribution in the flame at different conditions. The results show that the increase in initial temperature can improve the reaction rate, shorten the ignition delay time, and increase the flame combustion intensity and speed, because of the earlier evaporation and pyrolysis process in the RDX samples. Increasing the initial temperature also enhances the thermal effect of the flame, which is related to the generation and consumption of NO to a certain extent.

**Keywords:** RDX; combustion; thermal radiation; NO chemiluminescence; optical diagnosis



**Citation:** Yan, Z.; Song, C.; Li, Q.; Niu, Y.; Wang, J.; Huang, Z. A Study on the Effect of Initial Temperature on Combustion Characteristics of RDX Based on the Optical Diagnosis Methods. *Energies* **2022**, *15*, 2421. <https://doi.org/10.3390/en15072421>

Academic Editor: Léo Courty

Received: 14 February 2022

Accepted: 21 March 2022

Published: 25 March 2022

**Publisher's Note:** MDPI stays neutral with regard to jurisdictional claims in published maps and institutional affiliations.



**Copyright:** © 2022 by the authors. Licensee MDPI, Basel, Switzerland. This article is an open access article distributed under the terms and conditions of the Creative Commons Attribution (CC BY) license (<https://creativecommons.org/licenses/by/4.0/>).

## 1. Introduction

Cyclotrimethylene trinitramine (RDX) is an explosive with great performance. It has been widely used in the blasting field due to its capability of producing high specific impulse with less smoke generation, low toxicity, and low corrosion [1,2]. Moreover, with the development of modern warfare, RDX is also used as an important ingredient of mixed explosives, gun powder, and rocket solid propellants.

There has been a lot of research on material synthesis [3,4], performance evaluation [5], microscopic reaction [1,6], and the improvement of composite material [7] in recent years. Several factors are considered to influence the combustion and explosive performance, including the material itself and the conditions of temperature, pressure, electric field, etc. [8]. With the combat conditions and the surrounding environment becoming more complicated and changeable, the initial temperature has been identified as an important factor affecting the performance of materials. The powder or propellant may be heated during the process of storage, transportation, or utilization under the special conditions, such as the hot gun chamber of high-rate-fire guns, which leads to the unsatisfactory effect of the ignition and combustion. Moreover, temperature will change the shock sensitivity of explosives and further affect the explosive safety [9,10].

Some research has been conducted to understand the effect of temperature on the material properties of RDX. Most of these studies were carried out from two aspects of macro-combustion and micro-reaction. Atwood et al. [11] systematically compared the dependence of burning rate on initial temperature and pressure for several energetic materials, which shows that increasing the initial values of the two conditions can improve the burning rate. Yang et al. [7] fabricated a RDX-based microcellular combustible object, and evaluated the heat resistance by using a hot wall with the temperatures of 473, 523, 573,

and 623 K. Urtiew et al. [12] measured the pressure histories of the heated HMX (octahydro-1,3,5,7-tetranitro-1,3,5,7-tetrazocine)-based mixed explosives, and they observed that the shock sensitivity of HMX increases significantly when the crystal phase of HMX changes from  $\beta$  to  $\delta$  at 463 K. Zhao et al. [9] investigated the effect of temperature on shock initiation of RDX-based aluminized explosives. It was found that the decrease in the shock sensitivity is attributed to the binder softening for 298~383 K; however, the shock sensitivity increases when temperature rises up from 383 to 443 K because of the increasing sensitivity of RDX. Xiao et al. [13] studied the storage temperatures of 223, 298, and 338 K on explosion characteristics of RDX-based thermobaric explosives, and they pointed out that the low storage temperature leads to the temperature and volume of the fireball. Zenin et al. [14] measured the parameters of RDX combustion zones at a lower temperature (173 K) and different pressures.

Regarding the microreaction research, the methods of thermal decomposition and numerical simulation were always adopted. The thermal decomposition experiment is an important way to reveal the reaction process at special temperature [5]. A typical study was carried out by Khichar [15], where simultaneous thermal analysis experiments were conducted by employing TGA (thermogravimetric analysis), DSC (differential scanning calorimetry), and FTIR (Fourier transform infrared spectroscopy) to analyze RDX under three slow heating rates and atmospheric pressure. The processes of vaporization, mass loss, thermal decomposition, and the species evolution were studied. Strachan et al. [16] developed a reactive force field method with molecular dynamics and studied thermal-induced chemistry of RDX at various temperatures and densities. Mar et al. [17] numerically studied the effects of different initial mass, temperature, pressure, additives, and heat transfer coefficients on the combustion of RDX by adopting Yetter' gas phase mechanism [18]. Results show that the RDX ignition process tends to be shorter and the maximum of the combustion temperature rises when the initial temperature increases from 600 to 1100 K. Quantum mechanics investigation of thermal decomposition of RDX in liquid phase was performed by Patidar [1], and five reaction pathways of early ring-opening reactions were identified. Khichar et al. [19] developed a reaction mechanism describing liquid-phase decomposition of RDX, and the mechanism accuracy was validated with the experimental data of FTIR spectroscopy at the fixed temperatures of 538, 548, 558, and 568 K. Moreover, other work based on the phase transition, the crystal phase characteristics of RDX at different temperatures and extremely high pressures were studied in [20,21].

As seen above, the initial temperature has a practical effect on the application of energetic materials. Although some relevant studies have been conducted, most work cannot directly display the process of combustion, the evolution of flame morphology, and the two-dimensional distribution of thermal radiation. In terms of chemical reactions, most studies focused on the pyrolysis process and chemical reaction of RDX before ignition. Although it is very important to understand the reaction process of the material, there is a lack of research on the evolution of radical concentration after ignition, especially the effect of the initial temperature on the change of intermediate components in the flame. Additionally, this information has a profound significance to the understanding of the combustion reaction process, the judgment of the combustion performance, and the high efficiency and green application of energetic materials. With the rapid development of optical diagnostic technology, the contactless optical measurement method can not only quickly capture 2D field information and the reaction changes, but also avoid the interference with the flame [22,23]. Therefore, in this research, the RDX samples were ignited by a concentrated platform with the samples placed on a heating plate. This plate can be set at different initial heating temperatures (the temperatures below the melting point of RDX). The whole ignition and combustion process was recorded by a high-speed camera, an infrared camera, and an ICCD chemiluminescence camera. The effects of initial temperature on the RDX combustion characteristics were then evaluated and analyzed. This research can provide guidance for the safe and efficient use of energetic materials.

## 2. Materials and Methods

### 2.1. Materials

The Class 3 RDX sample used in this study was obtained from Gansu Yinguang Chemical Industry Group Co., Ltd, Baiyin, China. The purity of the RDX sample was 99%. A field emission scanning electron microscope (Tescan, Czech, MAIA3 LMH, Brno, Czech Republic) was used to obtain the morphology images of the samples. As shown in Figure 1, there were large differences in size and morphology between particles. The particle size ranged from micrometer to millimeter. The large particles were polyhedrons with obvious edges and corners, and the larger number of small particles were ellipsoids with smooth surfaces. The sample particles with  $50 \pm 0.1$  mg were paved into cylindrical tablets on a W slice before the experiments. The diameter of the tablet was 10 mm, and the thickness was 1 mm.

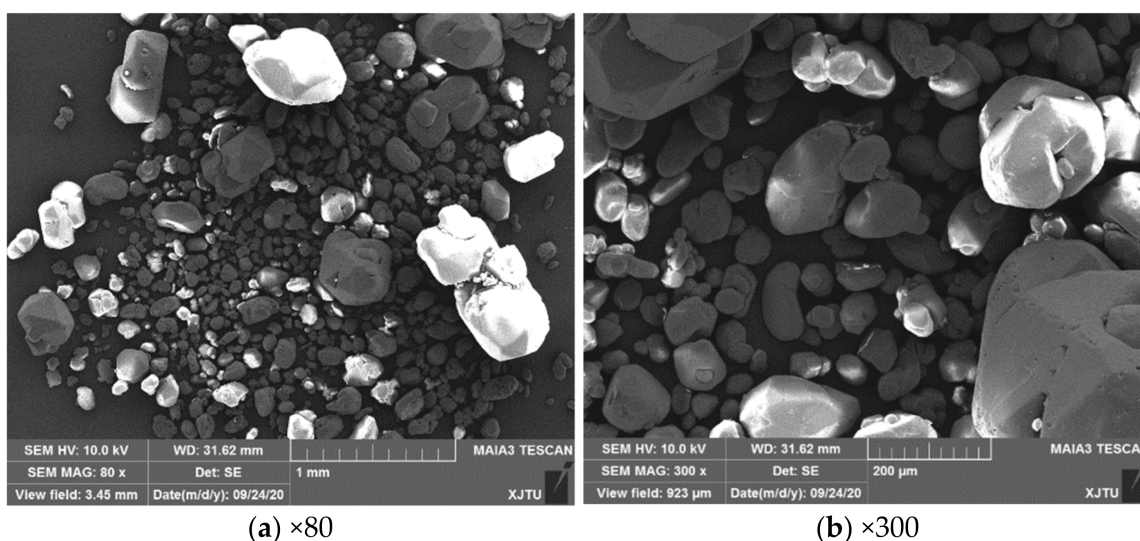


**Figure 1.** SEM images of the RDX sample under different magnifications. (a) The 80 times magnification and (b) 300 times magnification.

### 2.2. Devices and Methods

The experiment system is shown in Figure 2a, which includes ignition module, heating module, and signal control and data acquisition module. Because of good performance of non-contact ignition, the concentrated ignition device is always used to ignite solid materials [24].

As shown in Figure 2a, the ignition module contains a blower, a xenon lamp (AN-HONGDA, Shenzhen, China, AHD 3000 W), an ellipsoidal cold light mirror (Shenyang Academy of Instrumentation Science Co., LTD., Shenyang, China, E360), and a W slice. The mirror has two focal points: when a light source was placed in the first point of the mirror, and the light was focused at the second point. In the experiment, the xenon lamp with power value of 1900 W was placed in the first focal point, and then a hot point could be obtained at the second focal point position, where the W slice with RDX samples was set for ignition.

Under the W slice, the heating module was set, which includes an electric heating plate and a PID controller. The electric heating plate was fixed on a platform, which can provide the initial temperature only for heating the samples. In this study, the initial temperatures were 298, 323, 373, 423, and 473 K, respectively. These temperatures were all below the melting point of RDX.

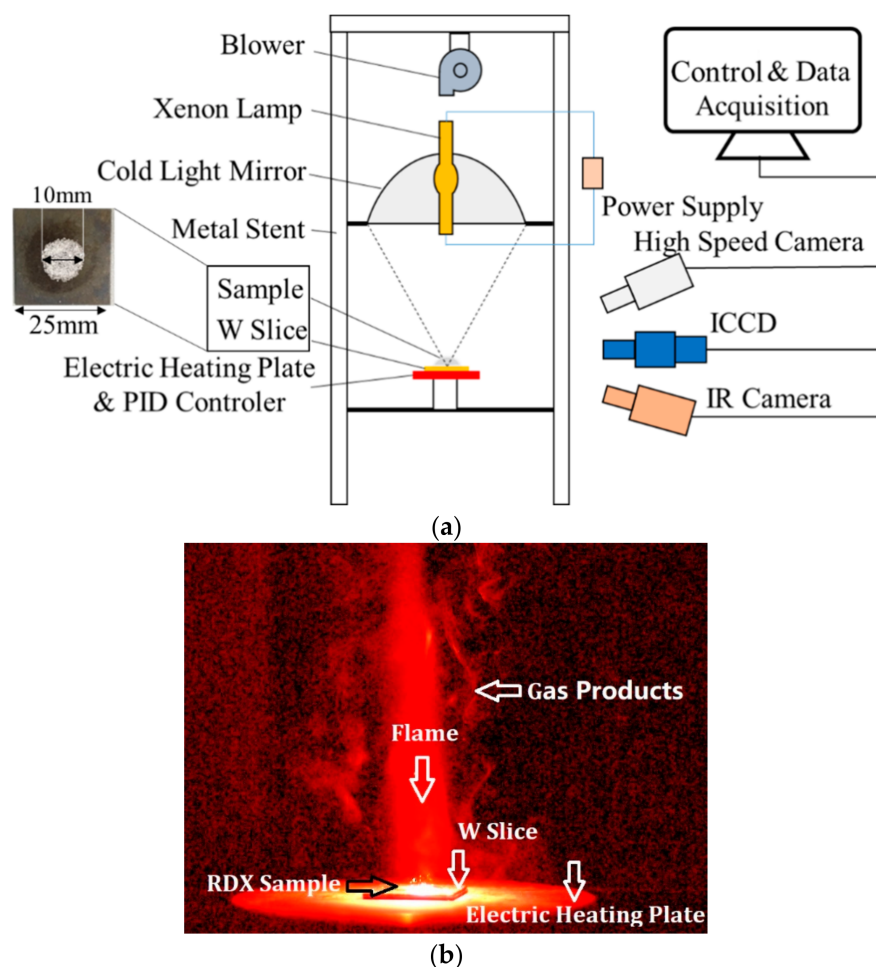


**Figure 2.** Setup of the experimental system and the flame structure. (a) Setup of experimental system; (b) Flame structure of RDX.

The signal control and data acquisition module includes three cameras and a computer. In the module, one is the high-speed camera (Ametek, New Jersey, America, Phantom V611), which can capture the combustion reaction process quickly. Its resolution, sample rate, and exposure time in the experiments were  $800 \times 600$ , 200 fps, and  $1 \mu\text{s}$ , respectively. The second camera is an ICCD camera (LaVision GmbH, Göttingen, Germany, LaVision Image Prox 2M) with DaVis 10 software for capturing the NO chemiluminescence using a NO filter (Center Wavelength = 248 nm, FWHM = 10 nm) [23], and the camera parameters contain the gain (70%), the gate ( $990 \mu\text{s}$ ), and the maximum frequency (21.28 Hz). Moreover, the thermal radiation could be utilized to distinguish the difference in the reaction temperature [13]. In the study, the radiation information was recorded by an IR camera (InfraTec, Dresden, Germany, 8855 hp) at 100 fps and  $640 \times 512$  pixels.

Before igniting the RDX, the electric heating plate was heated up to the initial temperature first. Secondly, the camera was turned on in advance for capturing the moment of the whole ignition and combustion process. Then, the W slice with samples was put on the heating plate. Ten seconds was waited to achieve a great heat conduction between the samples and the plate. Finally, the xenon lamp was turned on, and the reaction process and the combustion characteristics were recorded by the cameras. The flame structure is shown in Figure 2b. It is worth noting that the images captured by different cameras at the same time may have deviation because of the different frequencies of the cameras. However, it had little influence on the reaction process studied.

### 3. Results and Discussion

#### 3.1. Ignition and Combustion Process

The entire ignition process of RDX at 298 K was recorded by a high-speed camera, as shown in Figure 3. The ignition time was defined as the beginning when the xenon lamp was turned on. The whole process had four stages including melt, evaporation and decomposition, ignition, and the end of the reaction. Within 0–4 s, RDX solid particles were gradually heated as the xenon lamp was turned on. Experimental studies [3,25] showed that when the temperature of RDX is above 473 K, RDX is obviously endothermic, and the sample undergoes solid–liquid phase transition at this time. Meanwhile, Gao et al. [3] reported that some holes appear at the surface of RDX particle with increasing temperature. This indicates that the solid phase RDX also sublimates directly, resulting in the loss of mass. In the process of 4–10 s, as the temperature continued to rise; it can be seen from Figure 3 that a lot of gases gradually appear above the sample, because RDX in the liquid phase begins to evaporate and participates in the decomposition reaction at this time. Since the RDX molecule has a ring structure, five early ring-opening reactions have been identified by Patidar [1] in the decomposition process: (1) HONO elimination, (2) N-NO<sub>2</sub> homolysis, (3) reaction with NO, (4) autocatalytic decomposition via HONO and ONNO<sub>2</sub> addition, and (5) hydrogen abstraction via NO. RDX is gradually decomposed into N<sub>2</sub>O, NO<sub>2</sub>, NO, HCN, CH<sub>2</sub>O, CO, CO<sub>2</sub>, H<sub>2</sub>O and other small molecule gas phase products. During the process, a lot of heat is released, which further promotes the thermal decomposition reaction of the sample [19]. At 11 s, with the complete liquefaction of solid RDX, the pyrolysis reaction results in the accumulation of gas and liquid reaction products, and then a combustion behavior occurs in a high temperature environment. The combustion process was short and intense with obvious luminous and exothermic phenomena. With the rapid consumption of reactants, the whole reaction was finally completed, which is consistent with the reaction process described in the literature [26]. In addition, the long ignition delay time is mainly related to the ignition energy (the heating power of the xenon lamp) [24,27]. It is worth noting that a certain amount of gas was still generated after combustion. This may be because the focus point of xenon lamp was located in the center of the sample. Therefore, the temperature near the edge of the sample was relatively low, leading to the incomplete consumption of the sample.

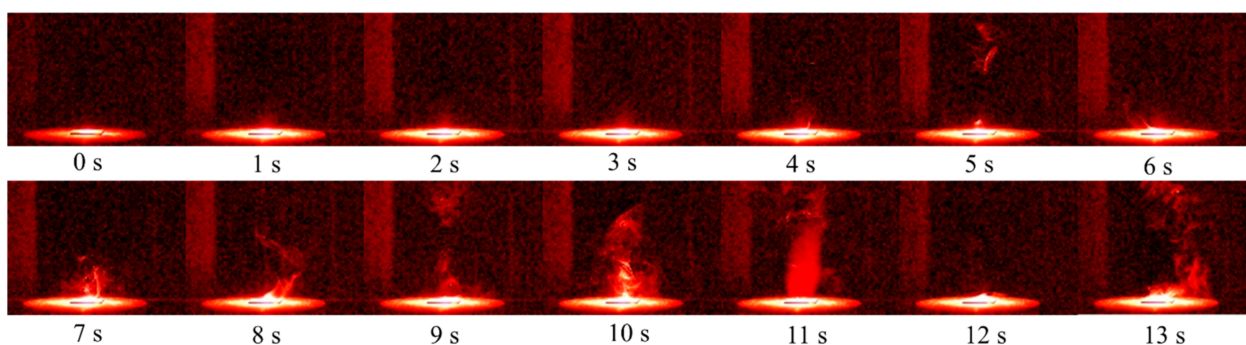


**Figure 3.** Ignition process of RDX at 298 K.

The ignition and combustion characteristics of RDX are the key properties concerned in the actual engineering application of the material. Figure 4 shows the flame development images of RDX at 298 K. Here, the beginning is defined as the moment when the fire core appears. The flame is divided into a development period (0–0.1 s), duration period (0.1–0.325 s), and decline period (0.325–0.475 s). In the development stage, it is observed that the fire core is generated in the gas phase region above the sample. Then, the flame rapidly develops upward through the reaction with the surrounding gas phase products, and the combustion intensity and flame brightness gradually increase. During the duration, the flame remains stable and the flame height fluctuates slightly. When the flame enters

the decline stage, the width of the flame root shrinks, the flame height and area decrease rapidly, and the brightness gradually declines and finally disappears completely.

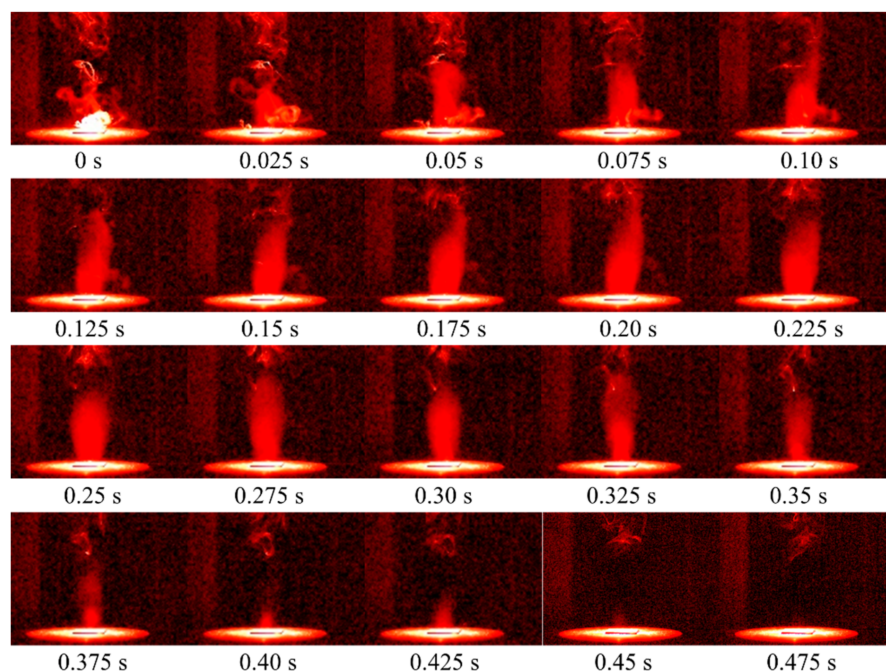


**Figure 4.** Flame development of RDX at 298 K.

According to the experimental and numerical simulation results, Volkov [26] and Liao [28] pointed out that the RDX gas and gas-phase decomposition zone are near the RDX burning surface. The RDX vapor can be rapidly consumed on the surface of the sample. For the combustion reaction mechanism of RDX, there are three steps [29]: (1) decomposition of RDX to  $\text{CH}_2\text{O}$ , HCN, and  $\text{NO}_2$  on the surface of the sample; (2) oxidation in the first stage to generate NO and  $\text{H}_2\text{O}$  and remove  $\text{NO}_2$ ; (3) oxidation in the second stage, HCN and NO are eventually converted to CO,  $\text{N}_2$ , and  $\text{H}_2$ .

### 3.2. Influence of Initial Temperature on the Ignition Process

The ignition process of RDX at five different temperatures was obtained, as shown in Figure 5. With the increase in the initial temperature, the generation of the gas phase products was earlier, indicating that the pyrolysis and evaporation processes were accelerated obviously. At the same time, it was also observed that the ignition delay time was significantly shortened. With the temperature increased from 298 to 473 K, the flame morphology changed from ellipsoid to conical shape, and the flame height increased. This all indicates that the increase in the initial temperature could promote the combustion intensity and combustion speed. Comparing the gas production before and after the combustion process, it was found that the gas production was similar at 423 K and below, while a lot of gas was obviously generated in the pyrolysis stage before combustion when the initial temperature was 473 K. This is because when the initial temperature is higher than 433 K, RDX particles begin to enter an obvious mass-loss stage [3]. After the xenon lamp was turned on, the sample quickly entered the evaporation and pyrolysis stage, and the rate was higher than that at other conditions. Moreover, the increase in initial temperature also caused the sublimation of particles in advance and the production of the gas phase RDX [3]. However, there was still a large amount of gas after combustion at 473 K, indicating that the incomplete and insufficient combustion may exist for RDX vapor at 473 K.

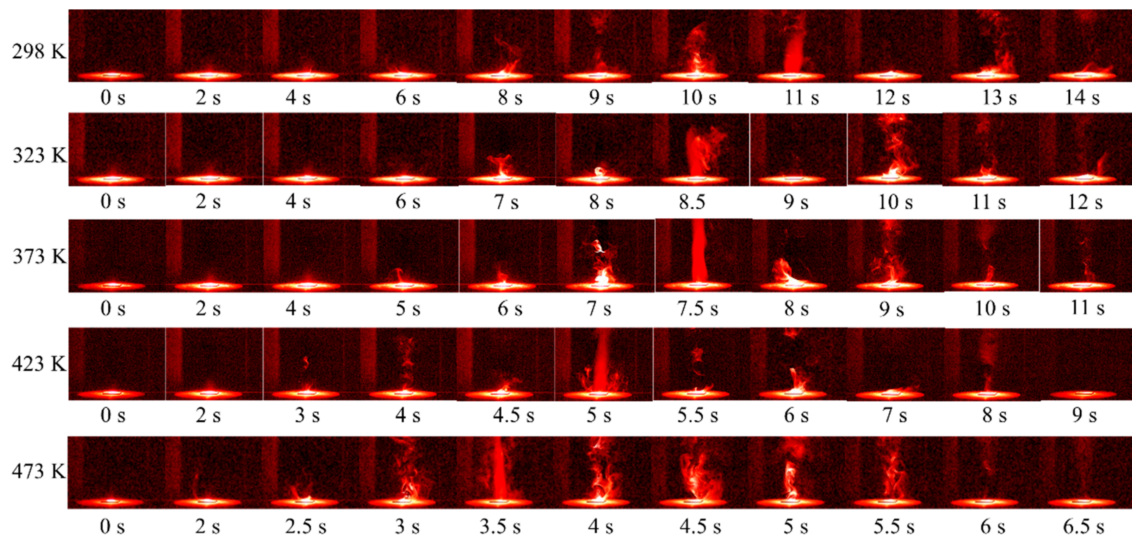


**Figure 5.** Ignition process of RDX at different initial temperatures.

The ignition delay time is defined as the period between the beginning and the time when flame core appears, and the combustion duration is defined as the period between the time when flame core appears and the time when flame core disappears. Then, these two combustion parameters of RDX at different initial temperatures were extracted, as shown in Figures 6 and 7. As seen in Figure 6, the ignition delay time decreased from 12.175 s at 298 K to 3.308 s at 473 K. Compared with 298 K, the ignition delay time at the other four temperatures decreased by 25.65%, 41.01%, 56.71%, and 72.83%, respectively, exhibiting an approximate linear decline. After ignition, the duration of combustion gradually shortened from 0.515 s at 298 K to 0.448 s at 473 K. Unlike the ignition delay time, the reduction degree of combustion duration is not so significant with increasing temperature. Compared with the condition of 298 K, the combustion duration at 323, 373, 423, and 473 K decreased by  $-0.65\%$ ,  $10.68\%$ ,  $14.89\%$ , and  $12.95\%$ , respectively. This indicates that the initial temperature contributes to the faster combustion speed, but the increment slows down as the temperature increases further. This is slightly different from the conclusion presented by Atwood et al. [11].

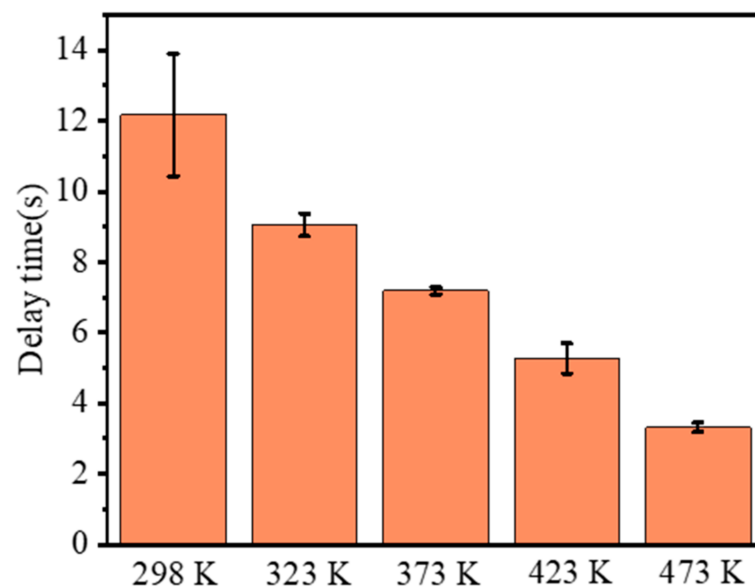


**Figure 6.** Comparison of ignition delay times at different initial temperatures.

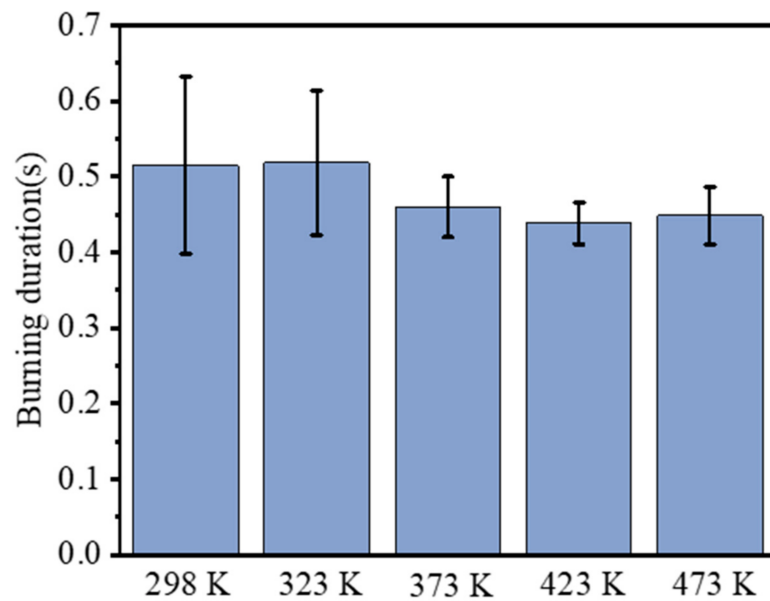


**Figure 7.** Comparison of combustion duration at different initial temperatures.

### 3.3. Flame Thermal Radiation

The thermal radiation of a flame is an important parameter for evaluating the combustion characteristics of energetic materials and providing a reference for developing the application criteria of materials at different conditions and scenarios. In this work, an infrared camera with a frequency of 200 Hz was used to record the radiation characteristics of the flame at different initial temperatures, as shown in Figure 8. Due to the complex gaseous medium in the combustion process, the flame temperature could not be calibrated. The temperature displayed by the scale in Figure 8 is the temperature after the calibration by a solid phase metal plate, and the change of flame thermal radiation could be identified according to the change of the color bar.

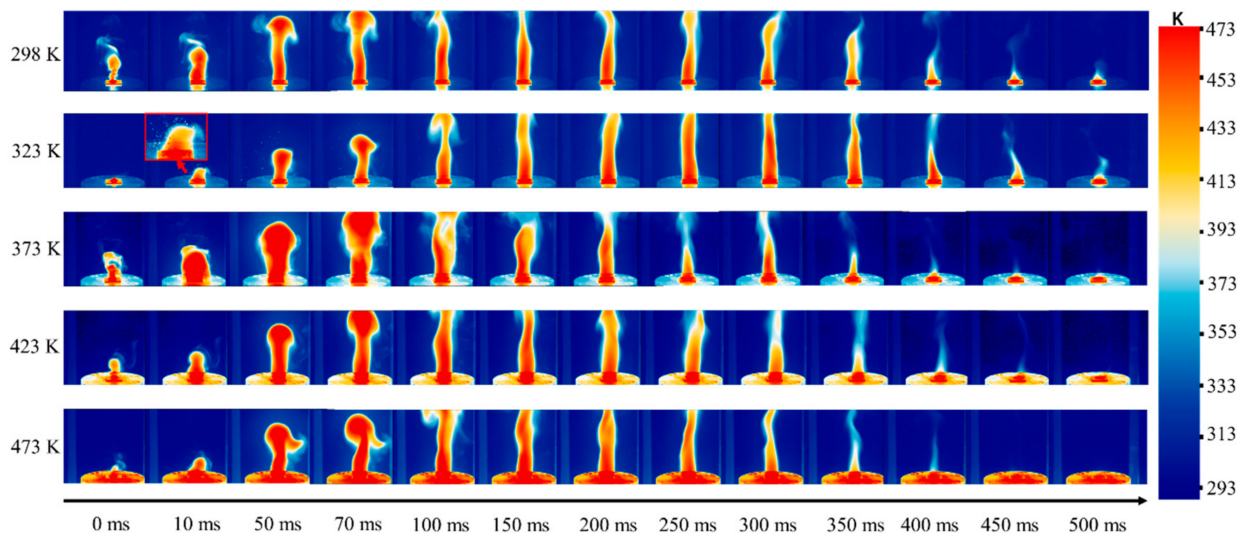


**Figure 8.** Flame thermal radiation at different initial temperatures (although the temperature is not the flame temperature, the change in color bar can represent the flame thermal radiation gradient).

When the initial temperature was 298 K, the thermal radiation increased gradually with the formation of the flame. From the radiation images, it can be clearly seen that there is an obvious mushroom head structure in the downstream of the flame when the time is 70 ms. In the development stage, the high thermal radiation signal is mainly located in the

upstream and downstream of the flame, indicating that the high temperature reaction zone mainly occurs in these two positions at the early stage. With the stability of the flame, the high temperature reaction zone is mainly located in the middle and upper zones of the flame, where the pyrolysis and combustion reactions of RDX continue [28]. In the primary heat release of the combustion process,  $\text{CH}_2\text{O}$  and  $\text{NO}_2$  react quickly to generate HCN,  $\text{H}_2\text{O}$ , NO, and CO. Subsequently, the conversion of HCN and NO to the final products is considered to be a dominant net reaction in the secondary heat release [27,29].

As the initial temperature rises, the flame becomes more intense during its generation and development. When the time was 10 ms at the temperature of 323 K, the obvious splashing phenomenon of particles was captured outside of the flame. It indicates that the micro-explosion occurs during the ignition process, and the generation of a large amount of gas leads to the ejection of some particles that are not involved in the reaction. The increase in the initial temperature also enlarged the mushroom heads in the flame at 50 and 70 ms. This phenomenon further confirms that the increase in the initial temperature accelerates the combustion rate and enhances the combustion intensity. In addition, it was observed that particle radiation could interfere with the maximum radiation signal in the flame, so the average thermal radiation signal of the whole flame area was extracted and the variation in the radiation signal was plotted with time at different initial temperatures, as shown in Figure 9. On the whole, the thermal radiation at each condition increased first and then decreased. With the increase in the initial temperature, the value of flame thermal radiation increased, which is consistent with the research of Xiao [13] and Mar [17]. Moreover, Xiao [13] pointed out that the increase in initial temperature can simultaneously improve the volume of flame, the thermal effect, and the pressure effect of the combustion process. This increase might be mainly related to the species concentration of two main heat release reactions, which are the primary oxidations of  $\text{CH}_2\text{O}$  and  $\text{NO}_2$  and the secondary oxidation of HCN and NO [29]. At the same time, at 373 K, the reason for the large radiation signal may be the change in the particle bulk density in the center of the samples when the ignition happens.

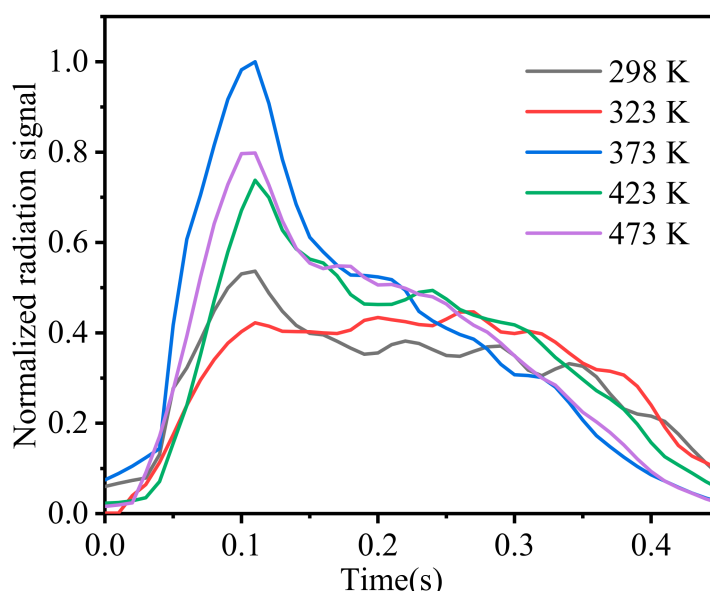


**Figure 9.** Variation in average thermal radiation signal in the flame with time.

### 3.4. NO Chemiluminescence Signal in the Flame

Exploring the evolution of NO concentration during the combustion process can not only aid the understanding of the combustion reaction, but also has a great significance for reducing NO<sub>x</sub> emissions and designing green propellants in the future.

The chemiluminescence method has been widely used in recent years to study species evolution in combustion process. Figure 10 shows the distribution of the NO chemiluminescence signal in the flames at different conditions. The distribution and development of NO in the flame can be seen. At 298 K, the overall signal intensity of NO experienced a process of first strengthening and then weakening. NO was mainly located in the inner center of the flame. Along the flame axis, the intensity of NO also increased first and then decreased, and the higher concentration of NO was closer to the root of the flame (the surface of the samples), which confirms the research results in the literature [26,28]. As mentioned in [29], NO is generated from the pyrolysis of RDX and the reaction of pyrolysis products ( $\text{CH}_2\text{O}$  and  $\text{NO}_2$ ) near the sample surface, and a large amount of heat is released at the same time, which is also the reason responsible for the high thermal radiation near the flame root. In the middle of the flame, the reaction of NO and HCN dominated with heat released, resulting in high thermal radiation and the rapid reduction in NO concentration. As the flame continues to develop downstream,  $\text{N}_2$ ,  $\text{H}_2\text{O}$ , CO, etc., are finally generated [29].

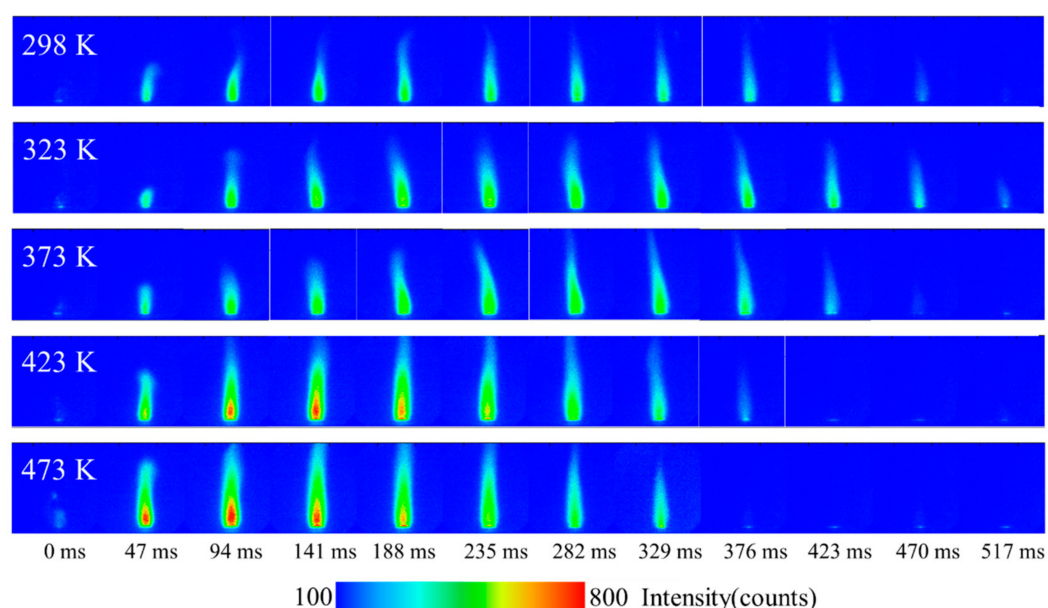


**Figure 10.** The distribution of NO chemiluminescence signal in flames at different times and initial temperatures.

The moment when the NO signal appears is defined as the beginning. The peak NO signal intensity in the flame was extracted using the LaVison software and plotted in Figure 11. Combined with Figures 10 and 11, it is clearly seen that with the increase in initial temperature, the NO generation area extended significantly. The peak NO signal intensity increased, and its occurrence time was earlier. This was because the increase in initial temperature led to the process of pyrolysis and the formation of more gas-phase RDX earlier, resulting in the generation of a large amount of  $\text{CH}_2\text{O}$ ,  $\text{NO}_2$ , and NO. Moreover, the reaction of  $\text{CH}_2\text{O}$  and  $\text{NO}_2$  produces NO and contributes to the increase and earlier appearance of the peak concentration of NO [19]. When comparing Figures 8 and 10, it is found that with the increase in the initial temperature, the synchronous advance of maximum NO signal and maximum thermal radiation signal is not observed. This is because the change in flame temperature is affected by complex chemical reactions, and the change in NO on the flame axis has a positive contribution to the flame temperature.

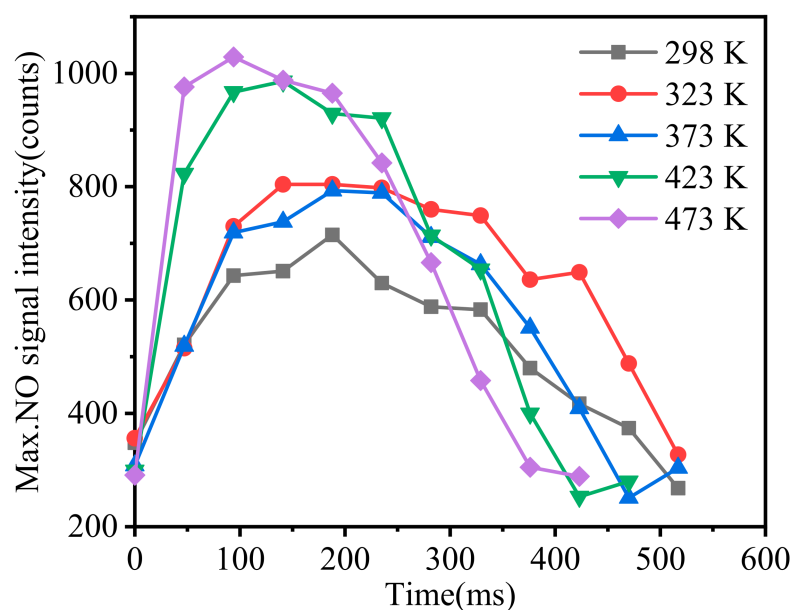


**Figure 11.** The variation in maximum NO signal intensity with time.

#### 4. Conclusions

In this work, the effect of initial temperature on the combustion characteristics of RDX was studied with different optical methods. The specific conclusions are as follows:

1. As the initial temperature of the sample increased, the evaporation and the pyrolysis processes appeared earlier, which reduced the ignition delay time, increased the combustion intensity and speed, and changed the flame morphology. When the initial temperature increased to 473 K, the gas production before and after combustion increased significantly.
2. Using an infrared camera, a mushroom head structure in the flame development stage was captured. The high thermal radiation signal was mainly located in the upstream and middle of the flame. The increase in initial temperature can enhance the thermal effect of the flame.
3. NO along the flame axis increased first and then decreased, and the high concentration of NO was always located in the upstream of the flame. With the increase in initial temperature, the peak NO signal increased, and the occurrence time was earlier. Both the generation and consumption of NO in the flame contributed to the thermal radiation.

**Author Contributions:** Conceptualization, Q.L., J.W. and Y.N.; formal analysis, Z.Y. and Q.L.; funding acquisition, Y.N., Q.L. and Z.H.; methodology, Z.Y. and C.S.; writing—review and editing, Z.Y. and Q.L. All authors have read and agreed to the published version of the manuscript.

**Funding:** This research was funded by Open Cooperation Innovation Fund Project of Xi'an Modern Chemistry Research Institute (Grant No. SYJJ33) and National Natural Science Foundation of China (Grant No. 51776163).

**Data Availability Statement:** The data presented in this study are available on request from the corresponding author (Q.L.).

**Acknowledgments:** Analysis Instruments in School of Chemical Engineering of Xi'an Jiaotong University is acknowledged for providing SEM analysis.

**Conflicts of Interest:** The authors declare no conflict of interest.

## References

1. Patidar, L.; Thynell, S.T. Quantum mechanics investigation of initial reaction pathways and early ring-opening reactions in thermal decomposition of liquid-phase RDX. *Combust. Flame* **2017**, *178*, 7–20. [[CrossRef](#)]
2. Kumbhakarna, N.R. Combustion analysis of RDX Propellant and Novel High-Nitrogen Propellant Ingredients. Master's Thesis, Pennsylvania State University, State College, PA, USA, 2014.
3. Gao, C.; Yang, L.; Zeng, Y.; Wang, X.; Zhang, C.; Dai, R.; Wang, Z.; Zheng, X.; Zhang, Z. Growth and Characterization of  $\beta$ -RDX Single Crystal Particles. *J. Phys. Chem. C* **2017**, *121*, 17586–17594. [[CrossRef](#)]
4. Liu, X.; Lin, Y.; Zhou, S.; Sheehan, S.; Wang, D. Complex nanostructures: Synthesis and energetic applications. *Energy* **2010**, *3*, 285–300. [[CrossRef](#)]
5. Fathollahi, M.; Mohammadi, B.; Mohammadi, J. Kinetic investigation on thermal decomposition of hexahydro-1,3,5-trinitro-1,3,5-triazine (RDX) nanoparticles. *Fuel* **2013**, *104*, 95–100. [[CrossRef](#)]
6. López-Munoz, C.; García-Cascales, J.R.; Velasco, F.J.S.; Otón-Martínez, R.A. An Energetic Model for Detonation of Granulated Solid Propellants. *Energy* **2019**, *12*, 4459. [[CrossRef](#)]
7. Yang, W.; Li, Y.; Ying, S. Fabrication, Thermoanalysis, and Performance Evaluation Studies on RDX-based Microcellular Combustible Objects. *Propellants Explos. Pyrotech.* **2014**, *39*, 568–573. [[CrossRef](#)]
8. Zilberman, S.; Albagli, D.; Katzir, A. Experimental Characterization of Transient Burning Properties of RDX-XLDB Propellant. *J. Propul. Power* **2013**, *29*, 305–312. [[CrossRef](#)]
9. Zhao, P.; Chen, L.; Yang, K.; Geng, D.; Lu, J.; Wu, J. Effect of Temperature on Shock Initiation of RDX-Based Aluminized Explosives. *Propellants Explos. Pyrotech.* **2019**, *44*, 1644. [[CrossRef](#)]
10. Garcia, F.; Vandersall, K.S.; Tarver, C.M.; Urtiew, P.A. Shock Initiation Experiments on the LLM-105 Explosive RX-55-AA at 25 °C and 150 °C with Ignition and Growth Modeling. *AIP Conf. Proc.* **2007**, *955*, 907–910.
11. Atwood, A.I.; Boggs, T.L.; Curran, P.O.; Parr, T.P.; Hanson-Parr, D.M.; Price, C.F.; Wiknich, J. Burning Rate of Solid Propellant Ingredients, Part 1: Pressure and Initial Temperature Effects. *J. Propul. Power* **2012**, *15*, 740–747. [[CrossRef](#)]
12. Urtiew, P.A.; Forbes, J.W.; Tarver, C.M.; Vandersall, K.S.; Maienschein, J.L. Shock Sensitivity of LX-04 Containing Delta Phase HMX at Elevated Temperatures. *Am. Inst. Phys.* **2004**, *706*, 1053–1056.
13. Xiao, W.; Chen, K.; Xing, H.D.; Wang, B.L. Effect of storage temperature on explosion characteristics of RDX-based thermobaric explosive. *J. Phys. Conf. Ser.* **2020**, *1507*, 022010. [[CrossRef](#)]
14. Zenin, A.A.; Finjakov, S.V. Characteristics of RDX combustion zones at different pressures and initial temperatures. *Combust. Explos. Shock. Waves* **2006**, *42*, 521–533. [[CrossRef](#)]
15. Khichar, M.; Patidar, L.; Thynell, S. Power, Comparative Analysis of Vaporization and Thermal Decomposition of Cyclo-trimethylenetrinitramine (RDX). *J. Propul. Power* **2019**, *35*, 1–10. [[CrossRef](#)]
16. Strachan, A.; Kober, E.M.; Duin, A.V.; Oxgaard, J.; Goddard, W.A. Thermal decomposition of RDX from reactive molecular dynamics. *J. Chem. Phys.* **2005**, *122*, 054502. [[CrossRef](#)] [[PubMed](#)]
17. Mar, M.; Gillard, P.; Courty, L. Numerical simulations of ignition and combustion of RDX mixed with gaseous additives. In Proceedings of the 25th International Colloquium on the Dynamics of Explosions and Reactive Systems, Leeds, UK, 2–7 August 2015.
18. Yetter, R.A.; Dryer, F.L.; Allen, M.T.; Gatto, J.L. Development of gas-phase reaction mechanisms for nitramine combustion. *J. Propul. Power* **2012**, *11*, 683–697. [[CrossRef](#)]
19. Khichar, M.; Patidar, L.; Thynell, S.T.J. Improvement and validation of a detailed reaction mechanism for thermal decomposition of RDX in liquid phase. *Combust. Flame* **2018**, *198*, 455–465. [[CrossRef](#)]
20. Dreger, Z.A.; Gupta, Y.M. Decomposition of  $\gamma$ -Cyclotrimethylene Trinitramine ( $\gamma$ -RDX): Relevance for Shock Wave Initiation. *J. Phys. Chem. A* **2012**, *116*, 8713–8717. [[CrossRef](#)]
21. Dreger, Z.A.; Gupta, Y.M.J. Phase diagram of hexahydro-1,3,5-trinitro-1,3,5-triazine crystals at high pressures and temperatures. *J. Phys. Chem. A* **2010**, *114*, 8099–8105. [[CrossRef](#)]
22. Zhang, W.; Wang, J.; Lin, W.; Guo, S.; Zhang, M.; Li, G.; Ye, J.; Huang, Z. Measurements on flame structure of bluff body and swirl stabilized premixed flames close to blow-off. *Exp. Therm. Fluid Sci.* **2019**, *104*, 15–25. [[CrossRef](#)]
23. Wang, Z.; Lin, Y.; Wang, J.; Zhang, C.; Peng, Z. Experimental study on NO<sub>x</sub> emission correlation of fuel staged combustion in a LPP combustor at high pressure based on NO-chemiluminescence. *Chin. J. Aeronaut.* **2020**, *33*, 550–560. [[CrossRef](#)]
24. Liang, D.; Liu, J.; Zhou, Y.; Zhou, J.; Cen, K. Ignition and combustion characteristics of molded amorphous boron under different oxygen pressures. *Acta Astronaut.* **2017**, *138*, 118–128. [[CrossRef](#)]
25. Li, C.; Yan, S.; Cheng, Y. Thermal decomposition kinetics of RDX by TG-DSC-QM S-FTIR. *Chin. J. Explos. Propellants* **2009**, *32*, 32–35.
26. Volkov, E.N.; Paletsky, A.A.; Korobeinichev, O.P. RDX flame structure at atmospheric pressure. *Combust. Explos. Shock. Waves* **2008**, *44*, 43–54. [[CrossRef](#)]
27. Tian, Z.; Zhang, Z.; Lu, F.; Chen, R.J.P. Explosives, Pyrotechnics, Modeling and Simulation of Laser-Induced Ignition of RDX Using Detailed Chemical Kinetics. *Propellants Explos. Pyrotech.* **2014**, *39*, 838–843. [[CrossRef](#)]
28. Liao, Y.C.; Yang, V. Analysis of RDX monopropellant combustion with two-phase subsurface reactions. *J. Propul. Power* **1995**, *11*, 729–739. [[CrossRef](#)]
29. Beckstead, M.W.; Puduppakkam, K.; Thakre, P.; Yang, V. Modeling of combustion and ignition of solid-propellant ingredients. *Prog. Energy Combust. Sci.* **2007**, *33*, 497–551. [[CrossRef](#)]